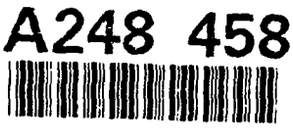

PSU TURBO 9201

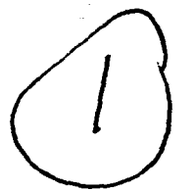

THE PENNSYLVANIA STATE UNIVERSITY
DEPARTMENT OF AEROSPACE ENGINEERING
TURBOMACHINERY LABORATORY

EXPLICIT NAVIER-STOKES COMPUTATION OF TURBOMACHINERY FLOWS

R. KUNZ
B. LAKSHMINARAYANA

January 1992

REPORT DOCUMENTATION PAGE

Form Approved
OMB No. 0704-0188

1. AGENCY USE ONLY (Leave blank)	2. REPORT DATE	3. REPORT TYPE AND DATES COVERED
	January 1992	Final Report Aug. 1, 1986 to Dec. 31, 1991

4. TITLE AND SUBTITLE
Explicit Navier-Stokes Computation of Turbomachinery Flows

5. FUNDING NUMBERS
DAAL 03-86-G-0044

6. AUTHOR(S)
R. Kunz and B. Lakshminarayana

7. PERFORMING ORGANIZATION NAME(S) AND ADDRESS(ES)
Department of Aerospace Engineering
The Pennsylvania State University
153J Hammond Building
University Park, PA 16802

8. PERFORMING ORGANIZATION REPORT NUMBER
PSU Turbo R 9201

9. SPONSORING/MONITORING AGENCY NAME(S) AND ADDRESS(ES)
U. S. Army Research Office
P. O. Box 12211
Research Triangle Park, NC 27709-2211

10. SPONSORING/MONITORING AGENCY REPORT NUMBER

11. SUPPLEMENTARY NOTES
The view, opinions and/or findings contained in this report are those of the author(s) and should not be construed as an official Department of the Army position, policy, or decision, unless so designated by other documentation.

12a. DISTRIBUTION/AVAILABILITY STATEMENT
Approved for public release; distribution unlimited.

12b. DISTRIBUTION CODE

13. ABSTRACT *(Maximum 200 words)*

A new three-dimensional explicit Navier-Stokes procedure has been developed for computation of turbomachinery flows. Several numerical strategies and modelling techniques have been developed and incorporated which enable convergent and accurate predictions of high Reynolds number flowfields across a wide range of Mach numbers. These include incorporation of a compressible low Reynolds number form of the turbulence transport model and other physical and solution parameters, eigenvalue and local velocity artificial dissipation scalings, a compact flux evaluation procedure and a hybrid low Reynolds number k-ϵ/algebraic Reynolds stress model. Detailed stability and order of magnitude analyses are performed on the discrete system of seven governing equations. Conclusions are drawn concerning the influence of system rotation and turbulence transport source terms, implicit source term treatment and the coupling of the discrete mean flow equation system to the turbulence model equations and its effect on the stability of the numerical scheme. Three-dimensional validation is provided by the results of an incompressible curved duct flow computation. A high Reynolds number axial rotor flow, for which extensive experimental data is also available, was computed. A backswept transonic centrifugal compressor flow, for which L2F meridional passage velocity measurements are available, is computed. Full Navier-Stokes solutions are presented which are shown to capture detailed viscous dominated flow features, including tip clearance and curvature induced and rotation induced secondary motions, with good accuracy.

14. SUBJECT TERMS	15. NUMBER OF PAGES
Computational Fluid Dynamics, Turbomachinery	221
	16. PRICE CODE

17. SECURITY CLASSIFICATION OF REPORT	18. SECURITY CLASSIFICATION OF THIS PAGE	19. SECURITY CLASSIFICATION OF ABSTRACT	20. LIMITATION OF ABSTRACT
UNCLASSIFIED	UNCLASSIFIED	UNCLASSIFIED	UL

EXPLICIT NAVIER-STOKES COMPUTATION OF TURBOMACHINERY FLOWS

Robert F. Kunz, Budugur Lakshminarayana
Pennsylvania State University

ABSTRACT

A new three-dimensional explicit Navier-Stokes procedure was developed for computation of turbulent turbomachinery flows. Several numerical strategies and modelling techniques were developed and incorporated which enable convergent and accurate predictions of high Reynolds number flow fields across a wide range of Mach numbers. These include incorporation of a compressible low Reynolds number form of the k-ε turbulence model in a fully explicit fashion, appropriate stability bound treatment of the transport turbulence model and other physical and solution parameters, eigenvalue and local velocity artificial dissipation scalings, a compact flux evaluation procedure and a hybrid low Reynolds number k-ε / algebraic Reynolds stress model.

This report provides a summary of this research. In what follows, primary research findings are summarized (details provided in cited references by the present authors), and several sample turbomachinery application results are provided. Specifically, two-dimensional results are provided for a supersonic compressor cascade operating at unique incidence condition. Three-dimensional validation is provided by a high Reynolds number axial rotor flow, for which extensive experimental data is available. This large scale computation is shown to capture rotational inviscid, blade and endwall boundary layer and wake flow physics, including spanwise mixing effects, with good accuracy. Finally, a backswept transonic centrifugal compressor flow, for which L2F meridional passage velocity measurements are available, was computed. Such flows are the most complex that exist in turbomachines. Full Navier-Stokes solutions are presented which are shown to capture detailed viscous dominated flow features, including tip clearance and curvature induced and rotation induced secondary motions, with good accuracy.

INTRODUCTION

Computation of viscous flows by numerical solution of the Navier-Stokes equations has become increasingly feasible due to improvements in numerical algorithms,

and to the ever-increasing speed and memory of digital computers. CFD codes available today are capable of calculating steady 3-D viscous flows about entire vehicles, and even unsteady viscous flows in 3-D turbomachinery stages. However, despite the rapid advance towards exploiting the power of computers now available, some serious limitations of these codes have yet to be adequately resolved. Surely the most profound of these limitations is the lack of accurate, general turbulence models. Secondary to this, but of much concern, is the role of artificial dissipation in Navier-Stokes calculations.

The purpose of this effort was to develop a new explicit, three-dimensional Navier-Stokes methodology for turbomachinery flow field prediction. In accordance with the need to address the items mentioned above, emphasis was placed on 1) incorporation of a low Reynolds number two-equation turbulence model in an explicit numerical solution procedure, 2) investigation of the role of artificial dissipation in the accuracy and stability of viscous flow computations on highly stretched grids. Also a comprehensive investigation of the stability of the procedure, including the influence of various geometric and flow field parameters on numerical stability, with emphasis on the turbulence model has been undertaken. Finally, simulations of a variety of complex two- and three-dimensional turbomachinery flows, across a wide range of Mach numbers, including a transonic centrifugal compressor, were performed, with the goal of using the flow solution to provide a detailed understanding of the viscous physical mechanisms in these machines.

An explicit numerical procedure of the Runge-Kutta class and a low Reynolds number form of the k-ε turbulence model was used in this work. Also, a hybrid low Reynolds number k-ε/high Reynolds number ARS model was developed and applied. One of the goals of this work has been to compute the flow in a centrifugal compressor. It was felt that for adequate resolution of the strong secondary motions in such machines, a low Reynolds number k-ε model would be significantly more appropriate than a mixing length model or a high Reynolds number form with wall functions. Application of the model adopted to the complex geometries in impellers, and all turbomachinery applications, is relatively straightforward. Additionally, as second order closures are adopted in the code, transport equations for k and/or ε need to be solved anyway, so the implementation, stability and application results presented in this report are directly relevant to incorporation of ARS and FRS closures.

The choice of an explicit numerical procedure in conjunction with a low Reynolds number k-ε model is not without its consequences. Specifically, nearly as well

documented as the accuracy advantages of using low Reynolds number form k-ε models over algebraic eddy viscosity models, are the perceived numerical disadvantages, and thereby the unpopularity, of implementing two-equation models in time-marching Navier-Stokes procedures. For these reasons, algebraic eddy viscosity models are often used to approximate the apparent stresses in CFD codes, since these models have little computational overhead and do not adversely affect the stability of the scheme. When transport models are used, the numerical stiffness associated with implicit and explicit computation of the Navier-Stokes and turbulence transport equations on the highly stretched grids required by low Reynolds number two-equation models has prompted researchers to adopt a variety of strategies to obtain convergent solutions. These include the use of wall functions, a hybrid approach (where an algebraic Van-Driest damping model is used to model the near-wall physics), and pointwise implicit source term treatment. These considerations have motivated the comprehensive stability investigation summarized below, in which the turbulence model is emphasized.

The explicit flow solver used for the numerical studies included in this report was written and developed by the first author and is described briefly here. The code is a structured H-grid, explicit, compressible, 3D, full Navier-Stokes flow solver which incorporates a compressible low Reynolds number k-ε model. Inlet characteristic boundary conditions, system rotation and periodic boundaries are available to accommodate turbomachinery applications. Euler and periodic boundaries consistent with either rectilinear or annular geometries are available. Eigenvalue and velocity artificial dissipation scalings are implemented. An algebraic Reynolds stress model which may be hybrid with the low Reynolds number k-ε model is available in the code.

The governing equations for the mean flow and turbulence models including the new hybrid k-ε/ARSM approach are provided in Ref. 1. Details of the spatial and temporal discretization procedures used are also available there. The remainder of this report is organized as follows: Analyses and conclusions regarding the artificial dissipation issues which arise in the high Reynolds number viscous flow computations of interest in this work are first summarized. Next, the results of stability and order of magnitude analyses of the seven discrete, numerically coupled governing equations are presented. The remainder of the report provides selected results of three Navier-Stokes turbomachinery calculations, with emphasis placed on the centrifugal compressor case. This report represents an extended summary of the first authors' Ph. D. dissertation which is included as the first of seven publications listed in the last section of the report, all related

to various aspects of the present research. Further details of individual topics are available in these references.

ANALYSIS OF NUMERICAL PROCEDURES

Two artificial dissipation issues of importance in high Reynolds number flow field computations were investigated. Two scaling functions which accommodate these considerations were studied. Details of these studies are available in Refs. 1, 2 and 4; a summary is provided here. An alternative flux Jacobian eigenvalue scaling was introduced and extended to three dimensions. This scaling reduces dissipation levels in the directions normal to grid stretching without increasing dissipation levels in the same direction as the grid stretching (nominally, the wall normal direction). It was found to be crucial to incorporate this anisotropic eigenvalue scaling in order that a converged three-dimensional rotor flow solution be obtained on a highly stretched grid. The role of artificial dissipation in corrupting solution accuracy in near wall regions, where physical diffusion is important, was illustrated. A local velocity squared scaling which tapers levels of artificial dissipation to zero near solid boundaries was introduced. It was demonstrated through numerical experimentation that it is crucial to incorporate this scaling in order that near wall physics be accurately resolved.

A comprehensive numerical stability analysis of the discrete, coupled system of seven governing equations was undertaken. Order of magnitude arguments were made for flow and geometric properties typical of internal flows, including turbomachinery applications, to ascertain the relative importance of grid stretching, rotation and turbulence source terms and effective diffusivity on the stability of the scheme. These studies were published in Refs. 1 and 3, where it was demonstrated through both analysis and corroborative numerical experiments that 1) it is quite feasible to incorporate, efficiently, a two equation k-ε turbulence model in an explicit time marching scheme, provided certain numerical stability constraints are enforced [Specifically, turbulence transport models, which provide large values of effective diffusion in regions where grid clustering may be high, give rise to dominant parabolic stability limitations, which must be incorporated in the numerical procedure]; 2) the role of source terms due to rotation on the stability of the numerical scheme is negligible for rotation numbers typical of turbomachinery flow calculations; 3) the direct role of source terms in the turbulence transport equations on the stability of the explicit numerical scheme is negligible, except in the earliest stages of iteration (a result which is contrary to that generally perceived); 4) there is no advantage to

numerically coupling the two equation model system to the mean flow equation system, in regard to convergence or accuracy; 5) for some flow configurations, including turbomachinery blade rows, it is useful to incorporate the influence of artificial dissipation in the prescription of a local timestep; and 6) explicit implementation of an algebraic Reynolds stress model (ARSM) is intrinsically stable provided that the discrete two-equation transport model which provides the necessary values of k and ε is itself stable.

Two other stability results, related to the numerical implementation of the turbulence model, were investigated and presented. Specifically, implicit treatment of the turbulence source terms did not improve the convergence rate of the explicit scheme. Additionally, terms which account for unstable, early iteration turbulence model behavior, arising from inviscid initialization procedures, were identified, and several stabilization procedures that the authors have found to be effective were presented.

SELECTED RESULTS OF TURBOMACHINERY APPLICATIONS

Turbulent Flow Through a Supersonic Compressor Cascade Operating at Unique Incidence Condition

A supersonic compressor cascade tested at DFVLR was investigated. Complete details of the experiment and computations is available in Refs. 1 and 2. The pre-compression blade was designed especially to investigate shock-boundary layer interaction with separation. At the test freestream Mach number, a standoff leading edge shock forms, which gives rise to a separated shock-boundary layer interaction aft of mid chord on the suction surface of the adjacent passage. Though the measured absolute inlet Mach number was supersonic, the blade row stagger angle was high so the axial component of the inlet velocity was subsonic. This gives rise to the "unique incidence" condition wherein there exists a fixed relationship between inlet Mach number and inlet flow angle. This phenomena as well as the complex wave interaction field within the passage and shock-boundary-layer interaction provide a challenging test case for both numerical scheme and turbulence model. Prediction of the unique incidence angle requires reasonably good resolution of both the leading edge geometry and the leading edge shock structure.

The computed case was experimentally tested in air at an inlet Mach number of 1.53 and a maximum attainable static pressure ratio of 2.13. The measured axial velocity density ratio (AVDR) of 1.02 indicated that the flow was close to two-dimensional. The Reynolds number based on chord was 2.7×10^6. As mentioned above, the inlet Mach number is supersonic, but axial velocity at the inlet to the computational domain is subsonic allowing left running characteristics to propagate out of the inlet plane. For this reason, subsonic inlet boundary conditions were specified : $p_o = 101325$ N/m^2, $T_o = 300$ K, $V_{\theta\infty} = 379.5$ m/s. At the subsonic exit plane the back pressure, $p_e = 56500$ N/m^2, was specified corresponding to the experimentally measured pressure ratio of the cascade, $p_2/p_1 = 2.13$.

A 129 x 100 computational grid was used for the Navier-Stokes calculation, which took approximately 6500 iterations to converge as measured by the invariance of total number of supersonic gridpoints in the field. This corresponded to approximately 40 minutes of CPU time on a Cray Y-MP.

In Figure 1a, a hand rendering of the shock wave pattern deduced from Schlieren visualization has been reproduced from the experimental investigation, alongside the computed shock wave pattern presented as divergence of velocity contours. The key features of the flow field are evident in this diagram, including the bow, lamda and passage shocks. In both experiment and computation, the bow shock is seen to impinge on the suction surface boundary layer of the adjacent passage. This gives rise to a lambda shock structure, a rapid thickening and separation of the boundary layer, and a Mach reflection which impinges on the pressure surface of the same passage. The high pressure ratio operating condition of this test case gives rise to a normal passage shock which impinges upstream of midchord on the pressure surface. This feature is also evident in both experiment and computation. The computation also shows some evidence of an oblique trailing edge shock, typical of supersonic compressor cascades at high operating pressure ratios.

In Figure 1b, the predicted isentropic blade surface Mach number is plotted against the experimental values. The calculation and experiment show fairly good agreement. The features labelled A, B and C in Figure 1b correspond to local compression regions where the bow shock impinges on the suction surface, the Mach reflection impinges on the pressure surface and the passage shock impinges on the pressure surface.

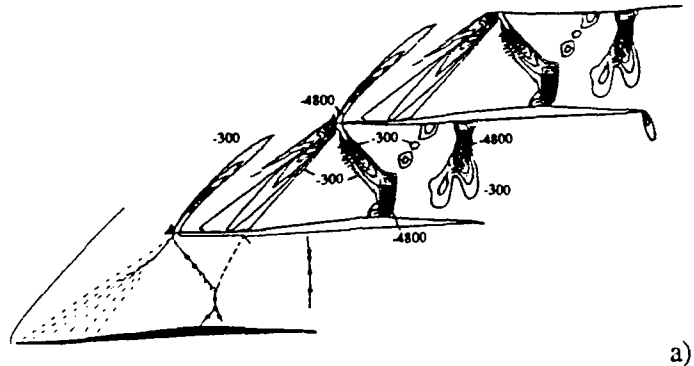

a)

b)

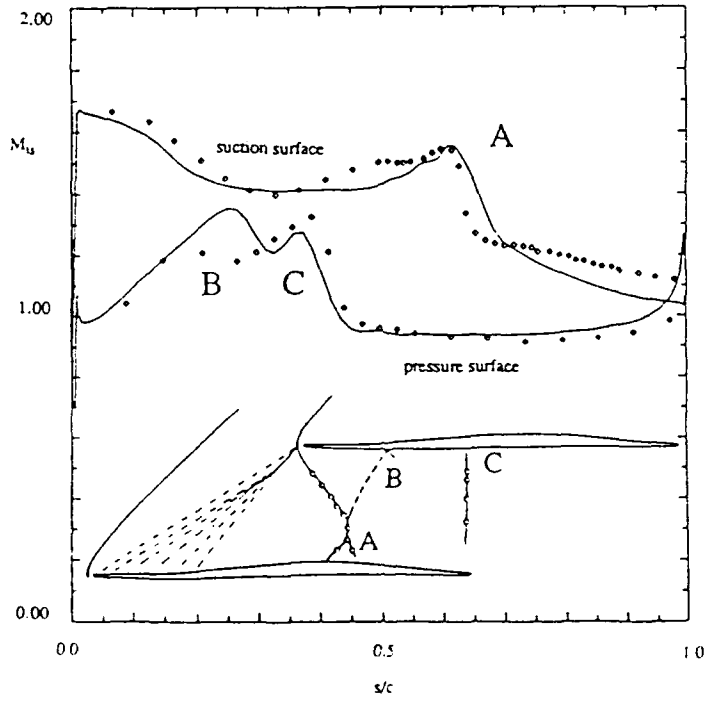

Figure 1. a) Shock wave pattern for PAV - 1.5 cascade. Divergence of velocity contours (-300 to -4800 by -500 [s^{-1}]). In this diagram, the top two passages show computed contours. The bottom passage is the shock wave pattern deduced from flow visualization and L2F measurements. b) Isentropic blade surface Mach numbers and shock structure identification for PAV-1.5 cascade computation. Calculated (solid line) and experimental values (symbols).

In Figure 2a, the computed total pressure ratio is compared with traverse probe measurements at an axial location 0.09 chord downstream of the cascade exit plane. The wake profile and loss distribution is reasonably well predicted, with the losses associated with the lambda shock system underpredicted. The wake centerline total pressure ratio is predicted reasonably well considering the difficulty in L2F measurement at this location.

Measured loss coefficients at maximum attainable cascade pressure ratio for a number of operating inlet Mach numbers were available. For comparison, the code was run at two additional operating points within the envelope of the experimental tests ($p_2/p_1 = 2.01$, $M_{inlet} = 1.45$ and $p_2/p_1 = 2.28$, $M_{inlet} = 1.58$). Figure 2b shows computed total pressure loss coefficients at all three operating points computed along with the envelope of experimental loss coefficients. Computed values lie within the envelope of experimental values.

Subsonic Compressor Rotor Operating at Peak Pressure Rise Coefficient

The code was utilized to predict the flow field in a subsonic rotor operating at peak pressure rise coefficient. Further details of the case are available in Refs. 1 and 4. The so called "Penn State Compressor Rotor" has a hub to tip ratio of 0.5 with an outer annulus wall diameter of 0.936 m. The rotor has 21 blades. The chord length increases from 0.124 m. at the hub to 0.154 m. at the tip. The blade stagger angle increases from 22.5° at the hub to 45.0° at the tip. The tip clearance was $\cong$ 3 mm.

The operating conditions for the computed case are as follows : flow coefficient, $\Phi = 0.50$, pressure rise coefficient (peak), $\overline{\Psi} = 0.55$, rotor shaft angular velocity, $\omega = 113\ s^{-1}$, tip velocity, $U = 53$ m/s. The Reynolds number of the flow based on chord length at midspan and rotor tip speed was 480,000.

An 89 x 45 x 45 (180225 points) computational grid was used for this calculation. In order to account for tip clearance flow, the grid was modified in the immediate vicinity of the shroud; a so-called "thin blade" tip clearance approach. The code converged in approximately 5000 iterations, which corresponded to approximately 10 hours on a Cray Y-MP.

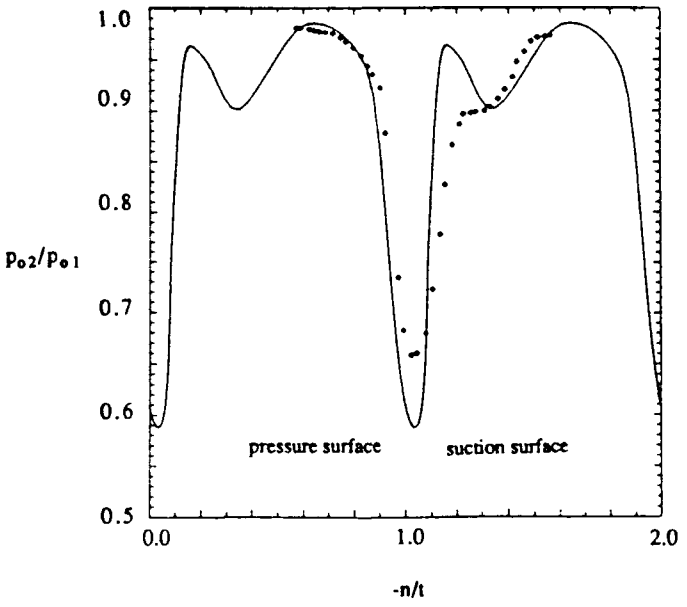

a)

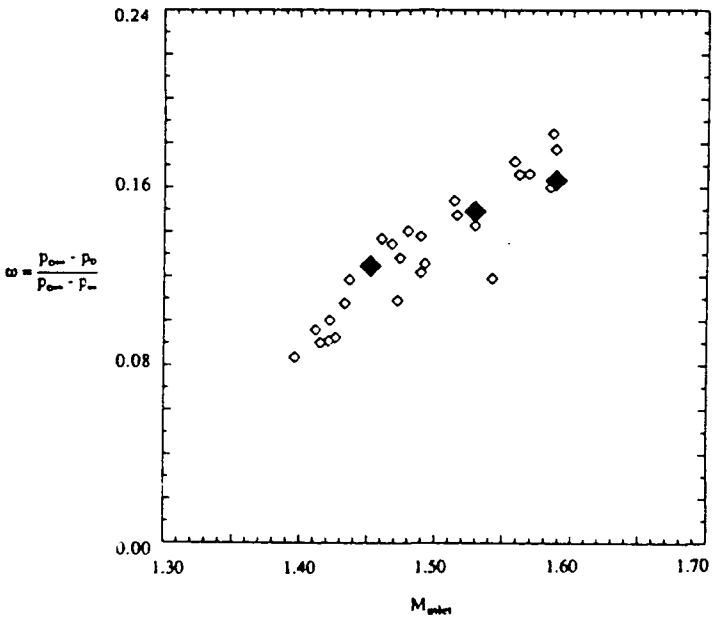

b)

Figure 2. a) Total pressure ratio profile 0.09 chord downstream of trailing edge for PAV-1.5 cascade computation. Calculated (solid line) and experimental values (symbols). b) Total pressure loss coefficients at several cascade operating points. Calculated (solid symbols) and experimental values (open symbols).

In Figure 3a, the blade to blade axial velocity distributions, obtained using LDV measurements at midspan, is presented with the Navier-Stokes predictions. The rotational inviscid flow features are seen to be well captured by the simulation, including immediately upstream of the leading edge where the presence of the blade gives rise to small velocity magnitudes due to the proximity of the stagnation point (inviscid effect).

Detailed blade boundary layer measurements were made for this operating condition, using a rotating hot wire. In Figures 3b and 3c, the predicted near-wall streamwise and radial velocity profiles are compared with measured values at midspan. The streamwise boundary layer velocity profile is captured with reasonable accuracy. It is noted that in the region $r/r_{tip} = 0.92 - 0.96$, the computations showed significant discrepancy (Ref. 4), in the near wall region. This is a region of large radial boundary layer transport interaction with the tip leakage and secondary flow, and is accordingly difficult to capture accurately with a Navier-Stokes simulation. The midspan radial velocity profiles are shown in Figure 3c. The agreement between experiment and computation again is good.

Five-hole pressure probe wake flow measurements are also available for this rotor flow. In Figures 3d, measured axial velocity profiles in the near and far wake are compared with computed profiles at midspan. Agreement between calculated and measured profiles is very good. The simulated wake thicknesses, centerline velocities and spreading rates are quite accurate.

In Figure 4a, spanwise distributions of circumferentially averaged axial velocity and absolute flow angle are presented at five downstream locations, ranging from the very near wake to the far wake regions. Agreement between experiment and computation is excellent except near the tip. The simulation captures well the radial distribution of these quantities through the extent of the wake. Also, the streamwise increase in V_x and decrease in absolute flow angle near both endwalls is captured.

In Figure 4b, the computed contours of relative stagnation pressure loss coefficient are presented for grid planes coincident with the blade trailing edge and the exit of the computational domain in the far wake. A number of interesting flow features are apparent in these plots. The loss contours at the trailing edge plane reveal

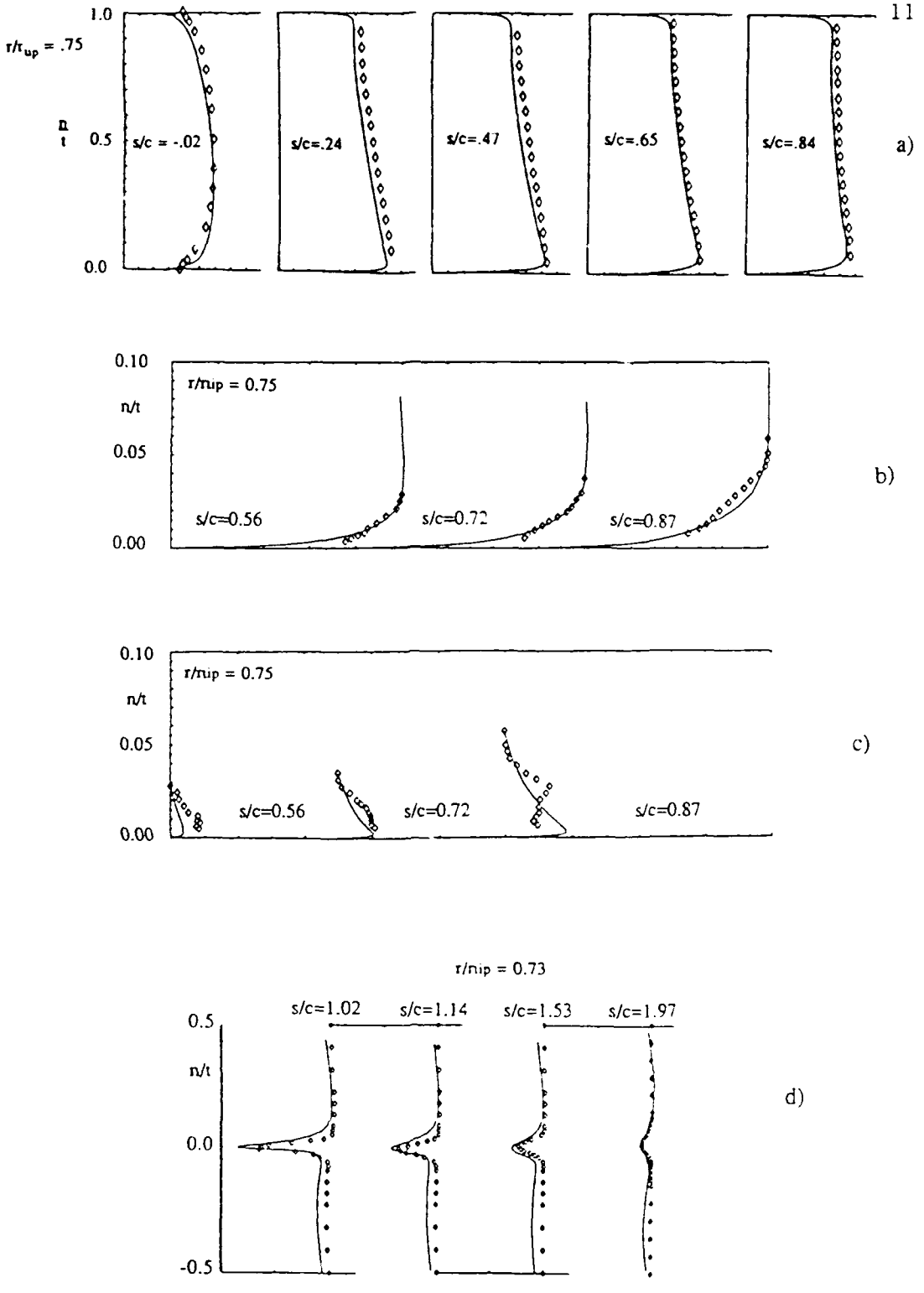

Figure 3. a) Blade to blade axial velocity distribution for PSU rotor flow, at midspan. Laser velocimeter measurements (symbols) and computed distributions (solid lines). b) Suction surface streamwise boundary layer velocity distribution at midspan. Rotating hot wire measurements (symbols) and computed distributions (solid lines). c) Suction surface radial boundary layer velocity distribution at midspan. d) Wake axial velocity distribution at midspan. Five hole probe measurements (symbols) and computed distributions (solid lines).

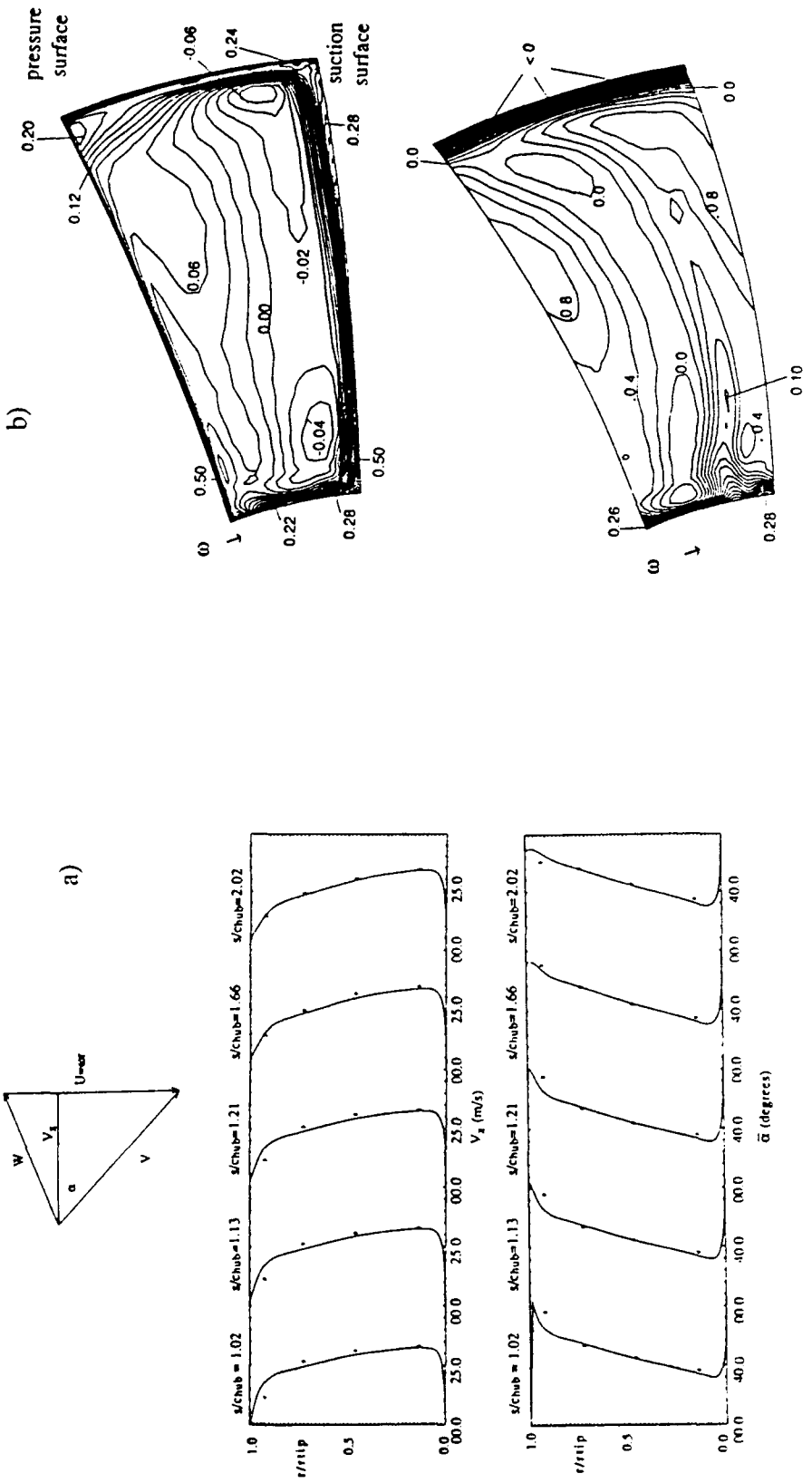

Figure 4. a) Passage averaged (mass weighted) values of axial velocity and flow angle downstream of PSU rotor passage. Averaged five hole probe measurements (symbols) and computed distributions (solid lines). b) Computed contours of relative stagnation pressure loss coefficient, $C_{p\,loss}$, at trailing edge, and exit plane of computational domain.

the presence of boundary layers near the blade surfaces where peak loss coefficients as high as 0.50 are predicted. The presence of secondary flow in the hub wall region and the resulting migration of low momentum fluid toward the suction side is indicated by the presence of a large loss region near the intersection of the suction surface and hub wall. The presence of high losses near the outer wall reveal the qualitative effect of leakage flow. The scraping vortex (of small radius) at the intersection of the pressure surface and the annulus wall is also captured qualitatively by the computation. The loss contours far downstream reveal an interesting phenomena related to spanwise and lateral mixing downstream of the blade row. The wake spreading decreases losses near the wake centerline and increases losses away from it. The effect of transverse mixing increases losses substantially everywhere except in the inviscid core region. The inviscid core region is located approximately in the middle third of the passage, where the losses are nearly zero. The corner flow loss region (at the intersection of suction surface and hub wall) has grown both in the blade to blade and spanwise direction. The radial velocities in the wake on the suction side have transported and elongated this loss region to higher radius. An interesting phenomenon is identified in the tip region of Figure 4b. Here the losses have not only decreased, but very close to the wall negative loss coefficients are predicted. This is caused by spanwise and lateral mixing due to wakes, leakage vortices and secondary flows.

Table 1. Comparison of Performance Parameters for Penn State Compressor Rotor

Flow Field Parameter	Measured	Computed	% Difference
Flow Coefficient, $\bar{\phi}$	0.50	0.495	1.0
Pressure Rise Coefficient, $\bar{\psi}$	0.55	0.563	2.4

Transonic Centrifugal Compressor Computation

The flow in centrifugal compressors and pumps provide one of the most challenging problems available to internal flow aerodynamicists. The complex three-dimensional physics in all of these machines has defied accurate prediction to date. The real flow in an impeller is drastically different from the desirable inviscid flow arising from the influence of curvature and rotation on rotor streamtubes in the absence of shear. A dominant boundary layer separation, or "wake" appears in many radial and mixed flow centrifugals, which alters strikingly the flow structure in the radial section of the impeller. A variety of strong secondary flows develop and interact due to the influence of centrifugal and coriolis forces on blade and endwall shear layers. Curvature and rotation also influence local turbulence intensity levels, thereby affecting the structure of developing boundary layers. Tip clearance flows and unsteady impeller-diffuser interactions introduce additional anomalies to an already complex passage flow. Additionally, there can be compressibility effects, even shock surfaces in the passage. Regions of flow reversal can be present at off design operation. In short, the complete physics involved are highly complex, and therefore, Navier-Stokes analyses to date have provided only qualitative accuracy.

The present technique was used to compute the flow field within a modern transonic centrifugal compressor stage. The results were compared with available L2F meridional velocity measurements within the impeller passage, shroud static pressure measurements and overall performance measurements. First, solutions using the low Reynolds number k-ε model were obtained. The hybrid k-ε / ARS model was also used to compute this flow. A summary of this work is provided here, further details are available in Refs. 1 and 7.

The centrifugal compressor chosen for detailed computational study was designed and tested at DFVLR. The low specific speed impeller (N_s = 80) has 24 blades and a 30° backsweep. The diffuser flow field was also computed. The design point was chosen for the present calculations. The flow parameters corresponding to this operating condition were : mass flow rate = 4.0 kg/s (.167 kg/s each passage), maximum inlet relative Mach number $\cong$ 0.8 (at shroud), machine rotation rate = 22,363 rpm, $p_{0,\text{diffuser exit}}/p_{0,\text{impeller inlet}} \cong 4.0{:}1$.

A 59 x 27 x 27 computational grid (43011 grid points) was used for the calculation.

Flow Field Calculation Using the k-ε Model

The first set of results obtained were for a solution obtained using the low Reynolds number k-ε model. For this run, the code converged in 5000 iterations, requiring approximately 2.5 CPU hours on a Cray Y-MP.

In Figure 5, circumferentially averaged shroud static pressure is plotted against time averaged static tap measurements. The agreement is very good except in the immediate vicinity of the impeller inlet, due most likely to the cusped leading edge, which is relatively thick compared to the blade spacing there.

Figure 6a shows normalized relative helicity contours at 65 % chord. The jet-wake structure is fully formed at this location. Evident are counter rotating secondary flow vortices. The tip clearance vortex is clearly distinguishable, and appears to have entrained some of the fluid from the pressure side half of the passage, "dragging" some high streamwise vorticity fluid towards the suction side. Meridional velocities compare quite well with experiment at this location, as shown in Figure 6b. The wake region near the shroud has been captured accurately. Most notable is that the experimental and computed wake flow has extended to midspan. The blockage that this fluid provides is seen to accelerate the higher momentum jet fluid towards the two blade and hub surfaces. Peak values of meridional velocity occur near the suction side-hub corner. These features are evident in the meridional velocity contours provided in Figure 6c, where it is also seen that the location of low meridional velocity near the shroud has migrated towards the suction surface.

Flow Field Calculation Using the Hybrid k-ε/ARS Model

In order to obtain some qualitative measure of the importance of Reynolds stress anisotropy on the flow field structure for this case, and to examine the numerical robustness of the hybrid model in flows where significant extra strain rates are present, the hybrid model was also used to compute the present impeller-diffuser flow field. Two runs

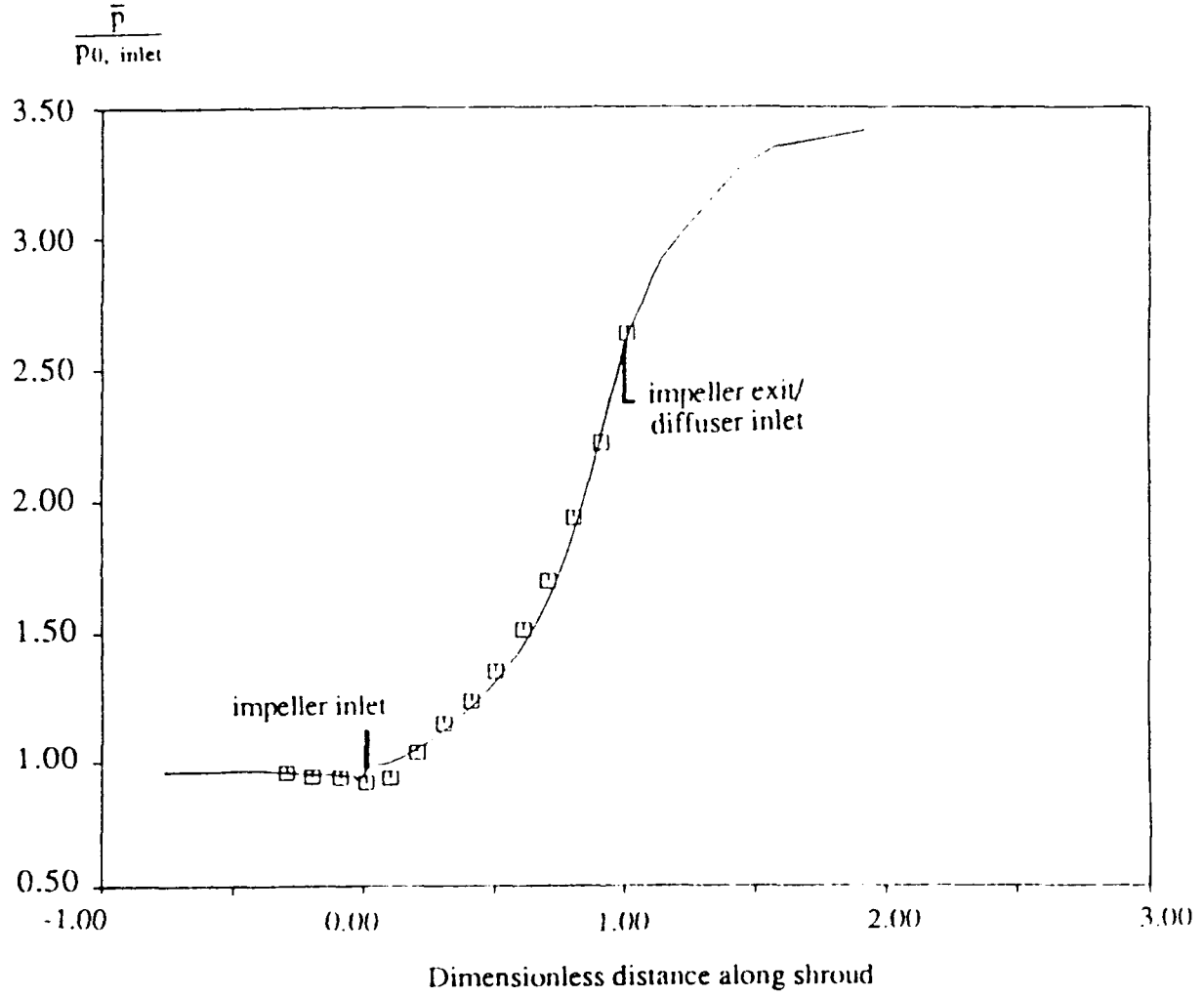

Figure 5. Shroud static pressure distribution. Experimentally obtained time averaged static pressure tap measurements (symbols), circumferentially averaged computed values (solid line).

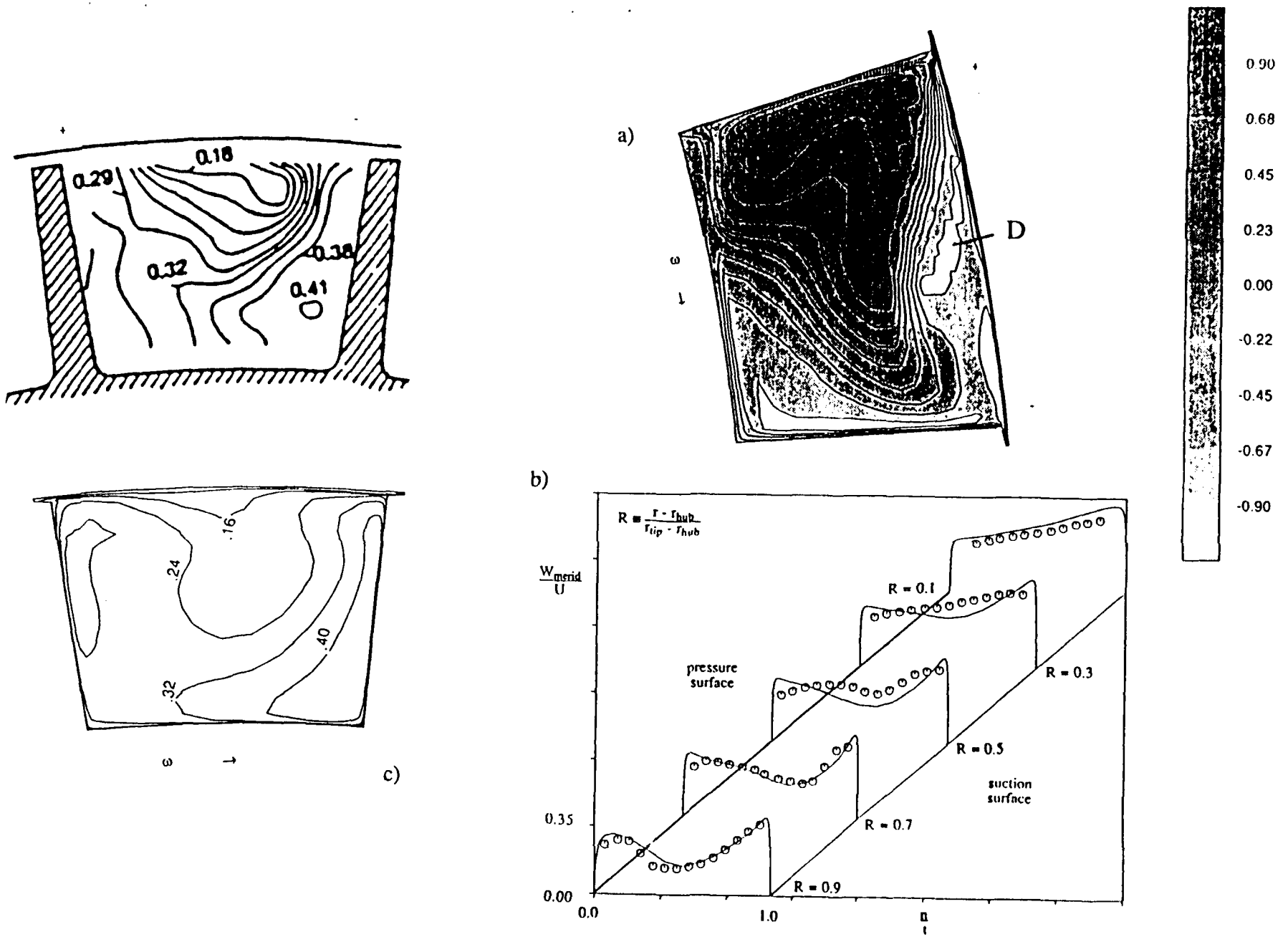

Figure 6. a) Computed normalized relative helicity contours, b) meridional velocity profiles [measured (symbols), computed (solid line)] and , c) meridional velocity contours [experimental (top), computed (bottom)] at 65% chord.

were performed using the ARSM model, one incorporating production by rotation terms R_{ij}, and one neglecting these terms.

Figure 7 shows converged meridional velocity profiles at 80% chord for the 1) k-ε (solid line), 2) hybrid, $R_{ij} = 0$ (long dash), 3) hybrid, $R_{ij} \neq 0$ (short dash) solutions. The meridional velocity profiles are seen to be very similar. It is noted however, that the near wall cross flow velocities and wall shear stress distributions were seen to vary substantially for the various models (Ref. 7). Table 2 compares predicted performance parameters between the three modelling approaches.

Table 2. Comparison of Performance Parameters for Transonic Centrifugal Compressor Stage

Mass Averaged Flow field Parameter	Measured	Computed (k-ε model)	Computed (k-ε/ARSM, $R_{ij} = 0$)	Computed (k-ε/ARSM, $R_{ij} \neq 0$)
Pressure Rise, $\frac{\bar{p}_{0,\text{ diffuser exit}}}{\bar{p}_{0,\text{ impeller inlet}}}$	4.00	3.80	4.01	3.92
Slip Factor, $\frac{\bar{V}_{\theta,\text{ impeller exit}}}{U_{\text{impeller exit}}}$	_	0.85	0.86	0.86

The slip factor, which arises due to coriolis "eddy"acceleration even in the absence of shear is seen to be negligibly affected by turbulence model choice. Predicted stage total pressure rise varies by as much as 5 % with different turbulence modelling.

As is clear from the foregoing results, the flow in this machine is very complex. As such, it is difficult in this case to make quantitative arguments as to the direct influence of the turbulence model on boundary layer structure. Specifically, it would be too bold to draw conclusions on precisely how local extra strains in the algebraic model directly influence local boundary layer structure, based on the results presented here. This is because local boundary layer physics, especially near the exit, are strongly dependent on the history of the entire developing passage flow.

What can be concluded from the results of this work are that extra strain rates are seen to influence the meridional flow physics only slightly, through local turbulence structure modification. Secondary motions, wall shear stress and total pressure rise

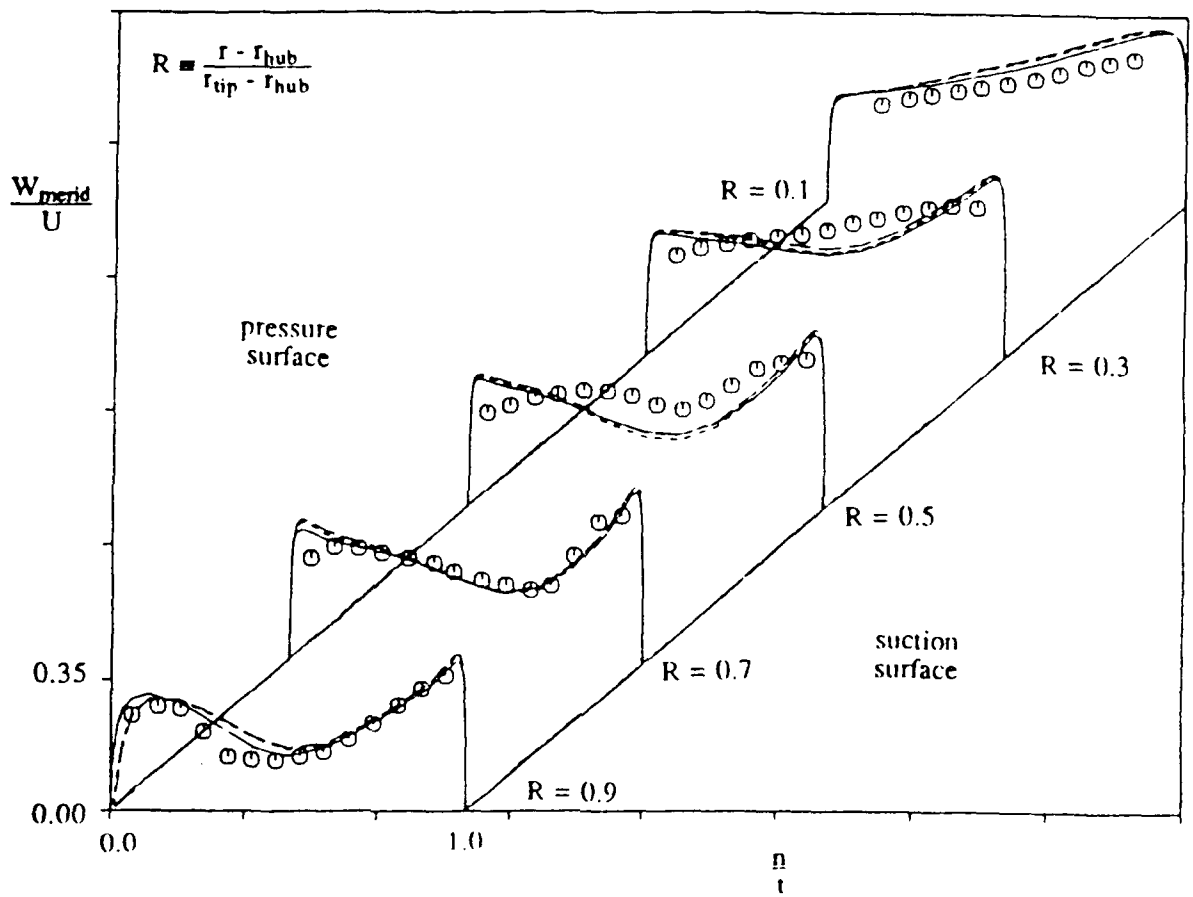

Figure 7. Meridional velocity profiles at L2F data acquisition Plane IV. Comparison of solutions using three turbulence models : low Reynolds number k-ε model (solid), hybrid model, $R_{ij} = 0$ (long dash), hybrid model, $R_{ij} \neq 0$ (short dash).

performance do show increased sensitivity to modelling choice. In the opinion of the authors, the proposed hybrid k-ε/ARS model is a sensible engineering approach to computing complex flows where strong extra strains are present. This approach is computationally efficient, reconciles the low Reynolds number k-ε form with the algebraic stress modelling, and seems to be numerically stable. However, further validation work is still needed, specifically the treatment of flows with isolated extra strain rates.

CONCLUSIONS

A new three-dimensional explicit Navier-Stokes procedure, which incorporates two-equation turbulence modelling has been developed and summarized in this report. Several analyses and techniques which have enabled convergent and accurate simulation of high Reynolds number turbomachinery flows on highly stretched grids have been developed and presented. These include extensive stability, order of magnitude and numerical verification studies applied to the discrete system of seven governing equations, with emphasis on turbulence modelling. Local velocity and flux Jacobian scalings of artificial dissipation operators were devised and applied. A hybrid low Reynolds number k-ε/high Reynolds number algebraic Reynolds stress model was developed. The procedure has been applied to a variety of turbomachinery flow fields, across a wide range of Mach numbers. The results of these computations were presented and interpreted, and indicated that the method provides accurate and convergent simulation of turbomachinery flow fields.

ACKNOWLEGDEMENT

This research was supported by the United States Army Research Office. The first author was supported by a USARO fellowship, through the grant DAAL03-86-G-0044, monitored by T. L. Doligalski. The authors also wish to acknowledge the National Science Foundation supported Pittsburgh Supercomputer Center (grants MSM 860009 P and CBT 90015 P) as well as the National Aerodynamic Simulation facility at NASA Ames Research Center for providing computer resources, through the course of this work.

LIST OF PUBLICATIONS BY THE PRESENT AUTHORS RELATED TO PRESENT WORK

1) Kunz, R. F., "Explicit Navier-Stokes Computation of Turbomachinery Flows," Ph. D. Thesis, Department of Aerospace Engineering, Pennsylvania State University, August, 1991.

2) Kunz, R. F., Lakshminarayana, B. "Explicit Navier-Stokes Computation of Cascade Flows Using the k-ε Turbulence Model," **AIAA Journal**, Vol. 30, No. 1, January 1992.

3) Kunz, R. F., Lakshminarayana, B. "Stability of Explicit Navier-Stokes Procedures using k-ε and k-ε/algebraic Reynolds stress turbulence models," **Journal of Computational Physics**, [Accepted for publication. To appear July, 1992].

4) Kunz, R. F., Lakshminarayana, B. "Three-Dimensional Navier-Stokes Computation of Turbomachinery Flows Using an Explicit Numerical Procedure and a Coupled k-ε Turbulence Model", **ASME Journal of Turbomachinery** [Accepted for publication. Originally published as ASME Paper 91-GT-146.]

5) Basson, A. H., Kunz, R. F., Lakshminarayana, B. "Grid Generation for Three-Dimensional Turbomachinery Geometries Including Tip Clearance," **AIAA Journal of Propulsion and Power** [Accepted for publication. Originally published as AIAA Paper 91-2360.]

6) Kunz, R. F., Lakshminarayana, B., Basson, A. H. "Investigation of Tip Clearance Phenomena in an Axial Compressor Cascade Using Euler and Navier-Stokes Procedures," **ASME Journal of Turbomachinery** [Recommended for publication by session chairman. To be presented at 1992 ASME Gas Turbine Conference.]

7) Kunz, R. F., Lakshminarayana, B., "Navier-Stokes Investigation of a Transonic Centrifugal Compressor Stage Using an Algebraic Reynolds Stress Model," AIAA Paper to be presented at the 1992 Joint Propulsion Conference.